

## CHAPTER 13

### Infragravity Waves in Storm Conditions

R. A. Holman, D. A. Huntley, and A. J. Bowen\*

#### ABSTRACT

Nearshore sediment is actively reworked during major storms, often significantly altering the nearshore morphology. It has been suggested that infragravity waves with wave periods 30-300 seconds are very important in the formation of major nearshore features.

A field study to further understand the nature of infragravity waves was carried out in Martinique Beach, Nova Scotia. Velocity measurements were taken using three electromagnetic flowmeters. Incident conditions varied from calm to swell and wind waves generated by hurricane Belle. Spectral analysis of the low tides revealed a sharp increase in the infragravity band energy associated with the storm. Throughout the storm the spectra of all three instruments were dominated by a strong 100 second peak which remained constant in frequency despite significant changes in the incident wave field. This peak is found to satisfy edge wave theory. A frequency selection mechanism based on longshore topographic trapping of edge waves is suggested.

#### INTRODUCTION

Surf beat, low frequency motion with wave periods of 30 to 300 seconds usually associated with shoaling waves, was first observed and christened by Munk (1949) and Tucker (1950). Their observations were relatively low amplitude (approximately 1/10 of the incident swell), which they explained as a modulation of a beating incident wave field with no longshore variability.

Gallagher (1971) modelled surf beat as edge waves with energy transfer from the incident waves through a non-linear mechanism. Huntley (1976) showed field evidence of a series of discrete, energetic infragravity (surf beat) peaks which he proved were edge waves.

Bowen and Inman (1971) suggest that natural, crescentic bars could theoretically be caused by edge waves. Reversing the logic, they then use the existence of crescentic bars to predict that narrow low frequency peaks of significant edge wave energy should exist on natural beaches. Suhayda (1974a, 1974b) presents field evidence which appears to confirm that standing infragravity waves generated perpendicular to the beach can lead to the formation of straight longshore bars.

\* Department of Oceanography  
Dalhousie University  
Halifax, Nova Scotia, Canada

Coupling this latter hypothesis that low frequency waves are closely related to major features with the common observation that these features undergo significant change under storm conditions (Schalk, 1963, Short, 1975) leads to the conclusion that surf beat probably forms an important part of the nearshore wave climate, especially during storms when one would expect to see narrow, strong peaks of low frequency energy. It is the purpose of this paper to present a field study of surf beat activity during incident conditions varying from calm to hurricane generated swell. Interestingly, a narrow 100 second peak is found to dominate the spectrum during storm conditions.

EDGE WAVES

Edge waves are normal modes of oscillation on a sloping beach. Eckart (1951) solved the shallow water equations for a plane beach of slope  $\tan \beta$  to find the velocity potential  $\phi$ , where

$$\phi = \frac{a_n g}{\sigma} f_n(x) \cos(ky - \sigma t) \quad \text{for a progressive edge wave} \tag{1}$$

and  $\phi = \frac{a_n g}{\sigma} f_n(x) \cos ky \cos \sigma t$  for a standing edge wave.

Here  $a_n$  is the shoreline amplitude of the edge wave of modal number  $n$ ,  $g$  is the gravitational acceleration,  $\sigma$  is the angular frequency,  $k$  the longshore wavenumber and  $t$  is time.  $x$ ,  $y$ , and  $z$  are a right-handed Cartesian co-ordinate set with  $x$  positive to seaward from the still water shoreline and  $z$  positive upwards from mean sea level. The off-shore behaviour is given by

$$f_n(x) = e^{-kx} L_n(2kx) \tag{2}$$

where  $L_n$  is the Laquerre polynomial of order  $n$ , having  $n$  zero crossings. Figure 1 is a plot of  $f_n(x)$  against the non-dimensional offshore distance  $\chi = \sigma^2 x / (g\beta)$  for the first four modes. The offshore profile of a standing incident wave is included for comparison. Edge waves must satisfy the dispersion relation

$$\sigma^2 = gk(2n+1) \tan \beta. \tag{3}$$

The onshore velocity  $u$ , longshore velocity  $v$ , and edge wave elevation  $\eta$  are given by

$$u = \frac{\partial}{\partial x} \phi, \quad v = \frac{\partial}{\partial y} \phi, \quad \eta = -\frac{1}{g} \frac{\partial}{\partial t} \phi \tag{4}$$

For a progressive wave at the shoreline, the ratio of  $u$  and  $v$  is simply

$$\frac{u}{v} = 2n+1$$

showing the dominance of  $u$  for higher modes.

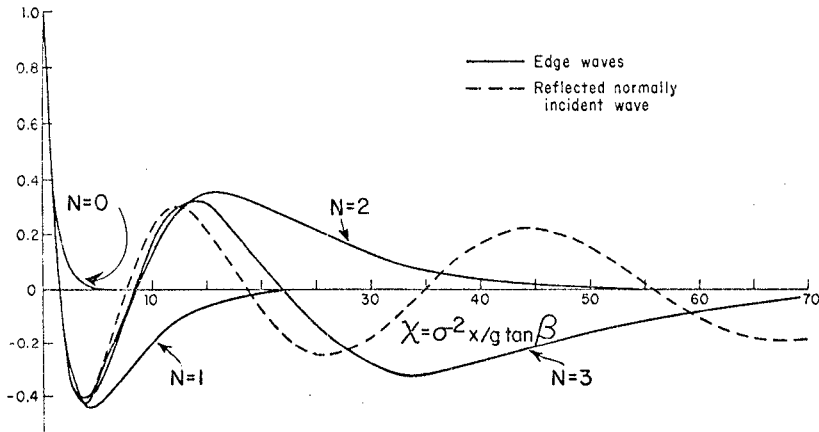


Fig. 1 Offshore dependence  $f_n(x)$  for edge wave modes 0, 1, 2, and 3, and or normally incident reflected wave.

#### EXPERIMENTAL

The site chosen for the field experiment was Martinique Beach, about eighty kilometers east of Halifax, Nova Scotia. Martinique has a fairly simple topography with an almost linear offshore profile of beach slope  $\beta = 0.02$ . The slightly concave shoreline is terminated at one end by a headland and at the other by a reef which extends 250 m offshore (figure 2). A second reef divides the length of the beach in the ratio 2:1. The beach has an open exposure to the Atlantic.

An array of sensors was set up along two ranges approximately 700 m from the west end of the beach (figure 3). The west range consisted of two Marsh-McBirney electromagnetic flowmeters labelled MMB1 and MMB2. One hundred meters to the east was a Cushing, spartype electromagnetic flowmeter labelled Cush. Sensors were mounted 50 cm above the sea bed.

All data was digitized at a 1/3 second interval prior to spectral analysis. Spectra presented will have two degrees of smoothing. A half filter width of 30 (HF=30), with a bandwidth of .0142 hz, was used to give a broad spectral picture (95% confidence limits are 0.75 and 1.4). For higher resolution a half width of 10 (HF=10), with a bandwidth of .0044 hz and confidence limits of 0.6 and 1.9, was used.

Four fifty minute data runs, centered at high, low, and both mid-tides, were usually taken per tidal cycle. Data was collected from the 6th to the 12th of August, 1976.

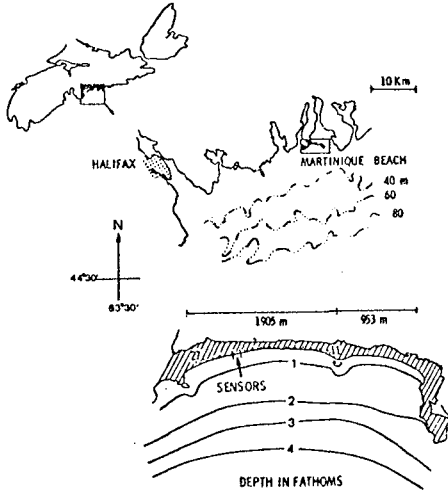


Fig. 2  
Location and plan view of  
Martinique beach.

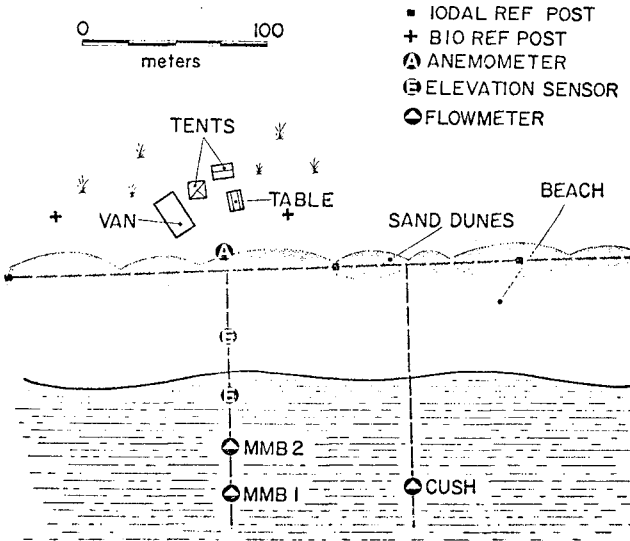


Fig. 3 Placement of sensors.

An overall summary of the visually observed wind and wave climate is shown in figure 4. Individual runs are indicated by stars with every fifth one numbered. Weather conditions changed through the week from four days of relative calm with low regular swell to winds of over 20 m/sec and accompanying high wave activity associated with the tail end of hurricane Belle which passed to the west (figure 5). Local winds were almost directly onshore at the height of the storm, shifting to the west during the decay. Rough visual estimates of significant wave height and significant wave period (figure 4) also reflect the presence of the storm, although the latter tends to underestimate the period of the spectral swell peak.

Figure 6 shows the mean run-up and visually estimated breakpoint for each run. Randomness of the incident waves and lack of an offshore length scale made breakpoint estimation difficult and introduced some scatter.

Beach profiles, taken at the beginning and end of the week, show a significant movement of sand during the storm (figure 7). This was also demonstrated by the partial burial of the two flowmeters in the west range.

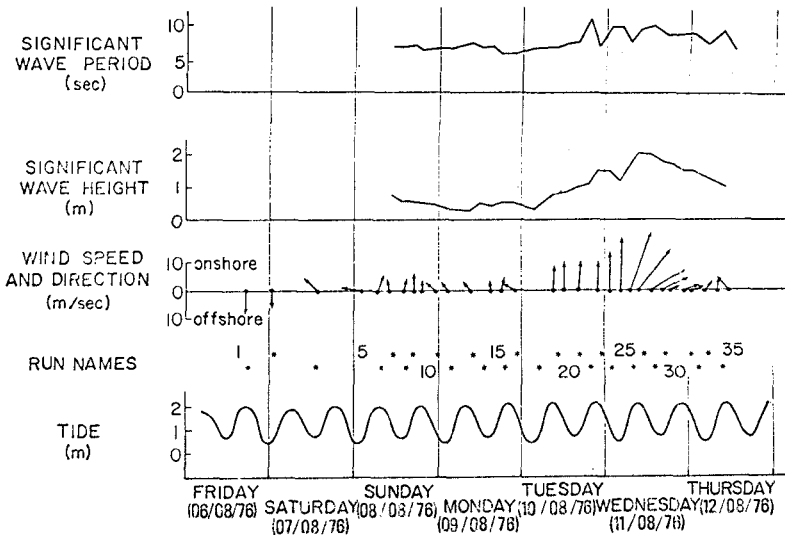


Fig. 4 Summary of the week of the experiment. Runs are indicated by stars with every fifth one numbered. The storm started in run 21, and peaked in run 26.

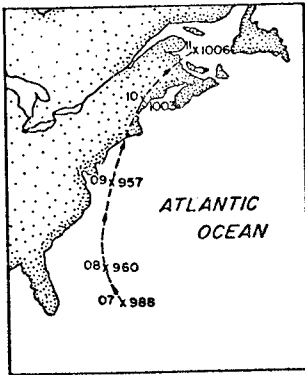


Fig. 5 Path of hurricane Belle. Numbers to left of x's indicate the day of the month, those of the right are barometric pressure.

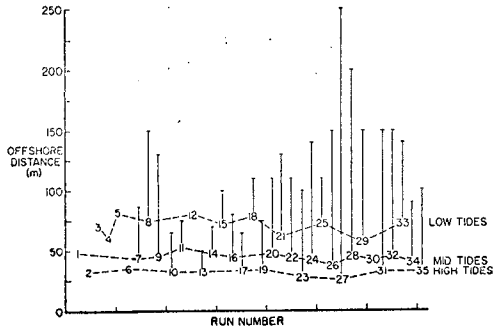


Fig. 6 Mean runup (numbers) and break point (short horizontal lines) for each run. Long vertical lines are then the surf zone width. There is no data for runs 1-6.

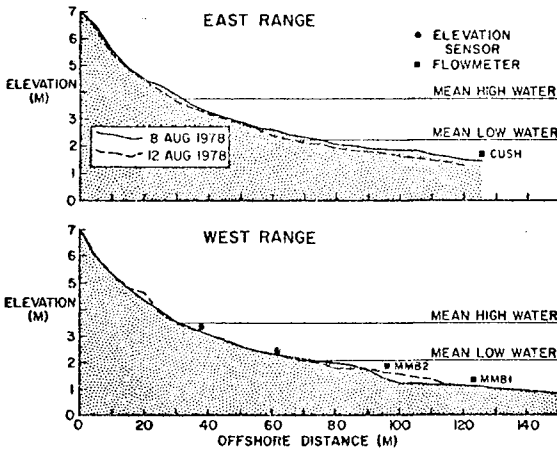


Fig. 7 Beach profiles before and after storm for both ranges. MMB2 was buried by the storm.

### RESULTS AND DATA ANALYSIS

Edge wave amplitudes dies away relatively rapidly offshore. Therefore, only the low tide runs, when the instruments are closest to the shore, will be considered in this paper.

Figure 8 shows the mean currents for each run. On/offshore currents are generally weak until run 21. MMB1 and MMB2 then jump to approximately 20 cm/sec offshore drift, staying offshore until the end of the experiment. The longshore currents change from a general westward drift during calm conditions to an eastward drift, the direction of travel of the storm waves, during the storm. Run 21 shows a longshore current divergence, with eastward flow at the east flowmeter and westward flow at the west range. This is consistent with a rip cell with rip heads slightly west of the west range and a larger distance east of the east flowmeter. Visual observations made by a diver during the run confirm this, reporting a rip current of approximately 50 cm/sec 15 m to the west of the west range.

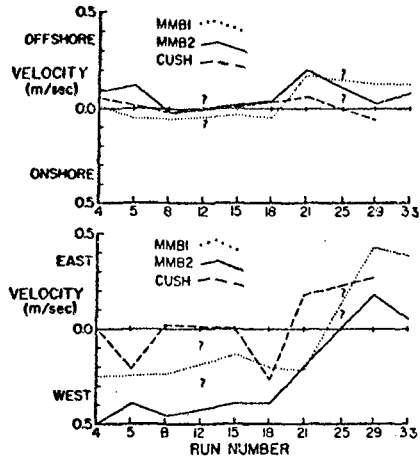


Fig. 8. Mean currents for the three instruments. Question marks indicate missing data.

Figure 9 shows a partial time series from run 29 just after the height of the storm. The longshore currents show substantial low frequency energy at a variety of time scales. The onshore currents show 100 second period activity particularly between 36 and 42 minutes. Evidence of shoaling can be seen from comparison of the on/offshore components of MMB1 and MMB2. MMB1 shows more of the variance contained in the higher frequencies (wind waves and swell), while the MMB2 shows relatively more variance in low frequencies. There is also some evidence of bore-bore capture, for instance at 42 minutes.

Figure 10 shows two spectra from the onshore channel of MMB2; run 12 is typical of calm conditions, while run 25 is at the height of the storm. The instrument is in the surf zone in both cases. Both spectra are fairly featureless with run 12 much flatter and of lower energy. The spectrum from run 25 is red up to a well-defined 100 second peak. Huntley and Bowen (1975) remark on the flatness of surf zone spectra when plotted on a log-linear scale. They are able to empirically parameterize the exponential decay coefficient,  $p$ , as a function of

local water depth  $h$  and wave amplitude at breaking  $a_b$ , as

$$p \propto h^{5/2} a_b^{-2}$$

Contrary to their result, this data shows  $p$  to vary as a positive exponent of  $a_b$  and a possibly negative component of  $h$ .

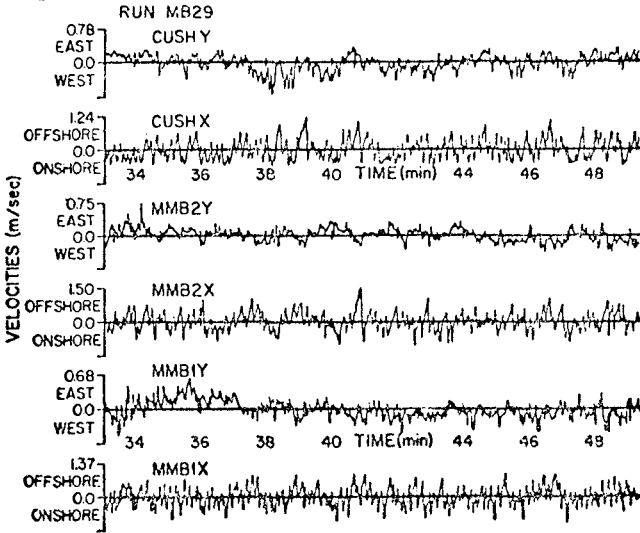


Fig. 9 Example time series for the three instruments. Run 29 is near the height of the storm.

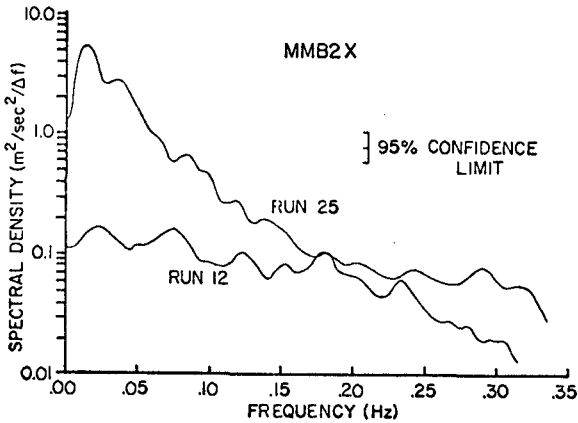


Fig. 10 Example onshore velocity spectra from calm conditions (run 12) and from storm conditions (run 25).

An estimate of the importance of the low frequency energy can be made by splitting the spectrum into a high frequency part consisting of swell, wind waves and higher frequencies, and a second part containing the lower frequencies. For run 29, the small dip in the spectrum at 0.075 hz is consistent with the low frequency side of the swell peak from the deeper MMB1 and is used as the division point. The low frequencies are found to account for 84% of the total energy for this run.

Picking a division point for run 12 is more difficult. Even using a relatively high value of .09 hz, the low frequencies account for only 41% of the total energy. Table 1 shows numerical comparisons between the calm run 12 and the stormy run 25. The mean square velocities were taken from the spectra in figure 10.

Table I. Comparison between calm and storm conditions.

Run ID	12 (calm)	25 (storm)
wind speed (m/sec)	1.5	21.2
significant wave height (m)	0.3	1.0+1.5
significant wave period (sec)	7.0	11.0
mean longshore current (m/sec)	-0.45	no data
Mean Square Velocities - MMB2X (all in $m^2/sec^2$ )		
low frequency	$1.2. \times 10^{-2}$	$1.86 \times 10^{-1}$
high frequency	$1.77 \times 10^{-2}$	$0.349 \times 10^{-1}$
total	$2.98 \times 10^{-2}$	$2.195 \times 10^{-1}$
% low frequency of total	41%	84%

Figure 11 shows time series of the spectra for the onshore and longshore components of the three flowmeters. Each heavy line represents an individual spectrum, from the first low tide, run 3, on the lower left of each plot, through to the last low tide, run 33, on the upper right. Each run is labelled above its y axis.

An obvious feature in the spectra is the presence of very low frequency energy in all longshore and many onshore spectra. Reduced smoothing fails to improve the detail of the energy. Because resolution is limited by run length, it can only be said that the low frequency hills are made up of energy from wave periods between about 3 and 200 minutes. Detrending largely removes periods longer than 200 minutes. Cross-spectral analysis between different channels of the

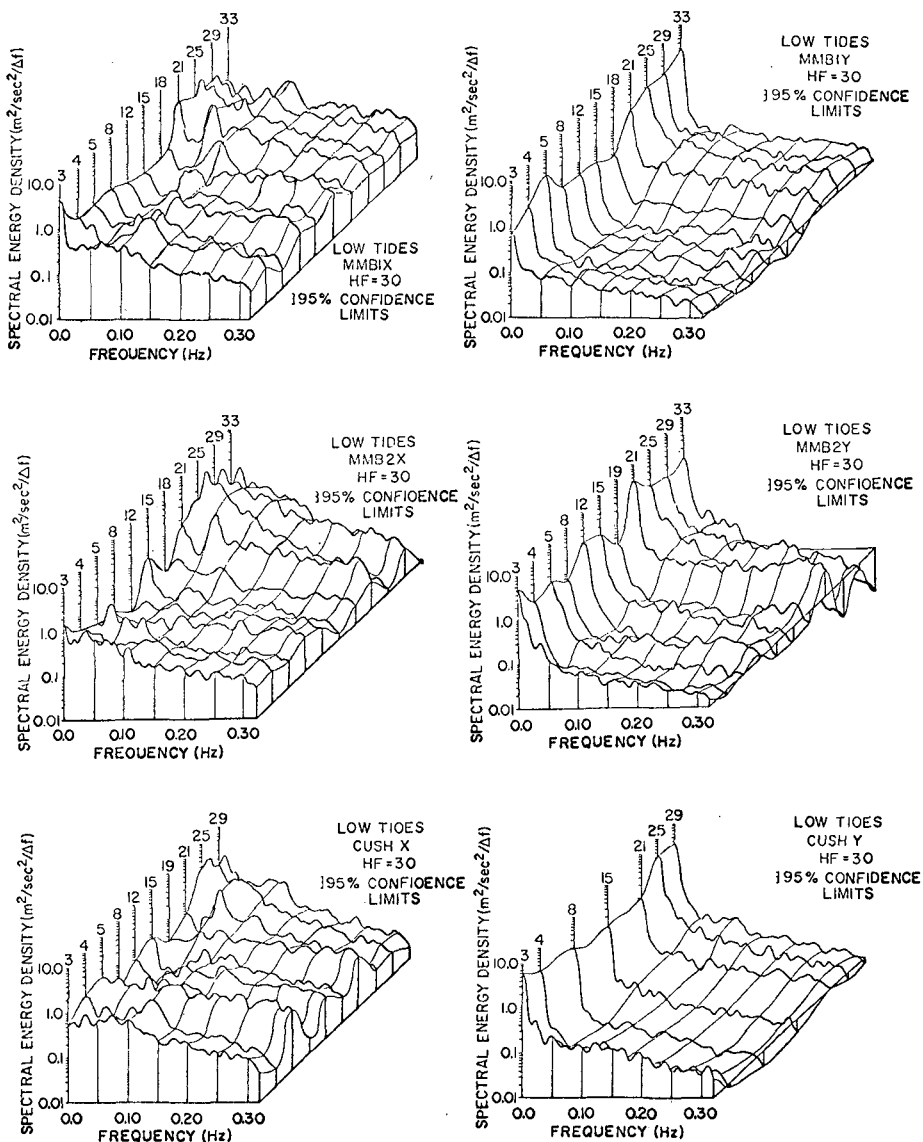


Fig. 11 Spectral time series for onshore and longshore velocities of all instruments. Each bold line is an individual spectrum with run numbers above the y-axis.

same instrument and between the same channels of different instruments reveals no pattern; coherences are usually insignificant. This implies a forced flow, not a free wave. One possibility is that the very low frequency energy may represent movements of the longshore current relative to the instrument.

The general trend of the week can be seen clearly from the spectral time series. The long calm period for the first half of the week is reflected by the low energies of the first seven spectra. The onshore component of MMB2, the shallowest instrument is, on average, featureless, while for MMB1 and Cush, a weak, unsteady wind wave peak is seen.

The forerunners of hurricane Belle appear in the onshore spectra of all three instruments on run 21 as an energetic swell peak of period 16 seconds and RMS velocity 14 cm/sec. This peak is then lost in the overall high energies of the shallow MMB2, but is seen to slowly shift to higher frequencies for MMB1 and Cush in agreement with expected wave dispersion.

Following the appearance of the storm forerunners in run 21 is a sudden, order of magnitude, increase in low frequency energy in the onshore velocity components of all instruments. In particular, for run 25, the spectra from all three instruments is dominated by a narrow, strong, 100 second peak. Throughout the rest of the storm, this peak continued to dominate the MMB2x and Cushx and stayed constant in frequency for all three instruments even though incident conditions changed significantly. (The peak seems to disappear for MMB1x. However, rerunning the spectra with decreased smoothing shows it to be present). For the MMB2x on run 25, the 100 second peak has a corresponding RMS velocity of 30 cm/sec.

Edge wave energy shows an offshore decay described by  $[\frac{\partial}{\partial x} f_n(\lambda x)]^2$  for the onshore velocity component. Since the instruments MMB1 and MMB2 were at different offshore distances on the same range, the ratio of the energies of the 100 second peaks could be compared to the theoretical ratio for edge waves of various modes. The observed ratios of 0.56 for run 25 and 0.36 for run 29 compare reasonably with the theoretical values for a mode 1 edge wave of 0.61 and 0.53 respectively, considering the difficulty involved in estimating a velocity from a spectrum. As can be seen from figure 1, the offshore energy decay for higher mode edge waves is quite similar to that of mode 1 for the small values of  $\chi$  involved ( $\chi \approx 1.5$ ).

Cross spectra between the onshore components of the different instruments were run with reduced smoothing. A peak which is highly coherent over the distance between instruments usually indicates a wave motion, while a peak which has only a low coherence is probably just a forced flow. Figure 12a shows spectra from the three instruments for run 29. The peaks at 100 seconds are quite narrow and consist in frequency from instrument to instrument. Figure 12b shows the

coherence and phase between the onshore velocity components of MMB2 and Cush. The 100 second peak shows up clearly with a coherence of 0.88 and a phase of 0±11 degrees. Cross spectra between other parts of onshore velocity components give similar results.

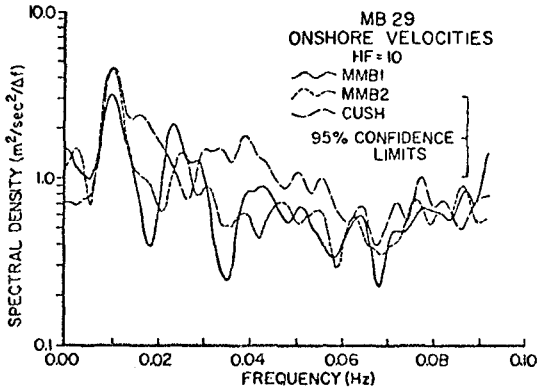


Fig. 12a Onshore velocity spectra for run 29 for the three instruments. Higher resolution is achieved by reducing the smoothing. The 100 second peaks stand out clearly in all three spectra.

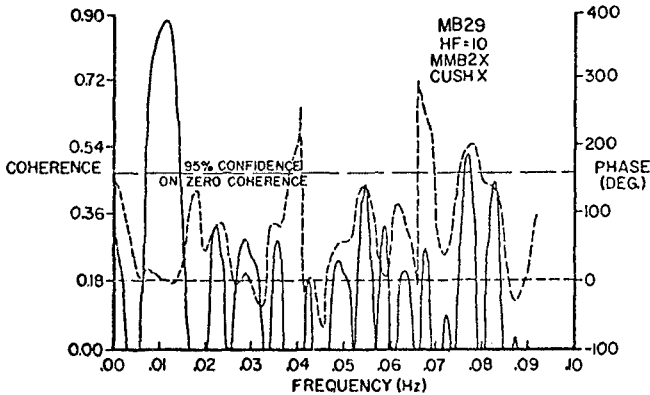


Fig. 12b Coherence and phase between the onshore velocities of the MMB2 and Cush for run 29. The 100 second peaks in figure 12a are seen to be highly coherent with a phase of 0°.

The corresponding 100 second peak is not present in the longshore spectra of MMB1 and Cush (figure 11) and only weakly present in that of MMB2, even with reduced smoothing to eliminate contamination from the very low frequency redness. Similarly, u-v cross-spectra fail to show significant coherence at 100 seconds. A possible explanation for this is shown in figure 13 which plots the offshore profile of the longshore velocity for 100 second mode 0, 1, and 2 edge waves (higher mode edge waves and standing incident waves are similar to mode 2). The positions of the flowmeters for runs 25 and 29 are superimposed on the figure. It is unfortunate that the zero crossing of longshore current for modes greater than 0 lies so close to the position of MMB1 and Cush. Even for run 25, a lower low tide, the longshore velocity at Cush is only 25% of the shoreline value, hence only 6% of the shoreline energy would be seen. The shallower MMB2 would see somewhat more energy, about 30% for run 25 and 10% for run 29. This may explain why MMB2 is the only channel on which the 100 second peak is seen.

For comparison, the onshore velocity component for a mode 1 edge wave is also plotted figure 13. The first zero crossing for this mode is well away from the instrument position. Coupled with this is the fact that the ratio of onshore velocity to longshore velocity at the shoreline goes as  $(2n+1)$  for progressive edge waves and  $(2n+1) \tan ky$  for standing edge waves. Thus, even for the worst case, MMB2 on run 25, the ratio of the onshore to longshore velocities for a mode 1 edge wave, as seen by the instrument, should be about 4:1 and the ratio of the spectral energies 16:1. For higher modes the ratio would be higher. This explains why the onshore peak can be so strong and the longshore peak so weak, and still be consistent with edge wave motion.

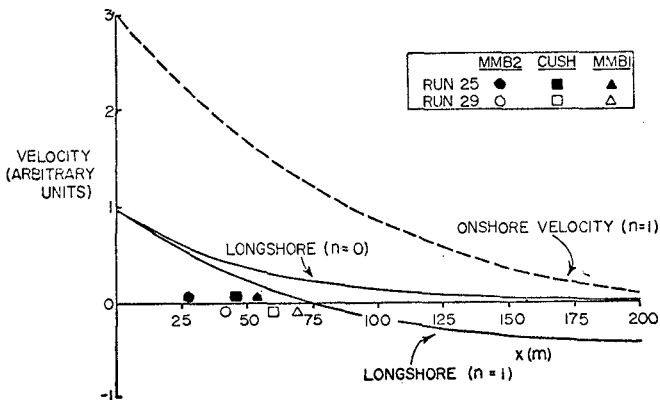


Fig. 13 Offshore behaviour of longshore current for a 100 second edge wave of mode 0, 1 and 2. The instrument positions for runs 25, 29 are included and are very close to the first node. This is not true for onshore velocity as seen from the mode 1 profile.

FREQUENCY SELECTION

The presence of energetic, low frequency waves, steady in frequency through a variety of hurricane-generated incident conditions, is important to the coastal engineer for the understanding of the growth of large beach features. However, there must be some underlying mechanism which provides the frequency selection either through forcing, damping, topographic constraints, or a combination of these.

The forcing mechanisms proposed by Longuett-Higgins and Stewart (1964) and Gallagher (1971) depend on beating in the incident wave field. This was tested directly by comparing the time series of the low-passed velocity and the incident envelope (the square of the high-pass record which is then smoothed). The correlation was not significant for the several time series tested, suggesting a broad banded forcing. However, it should be remembered that the time series tested were from within the surf zone where the strong non-linearities associated with breaking could have easily obscured the low frequency forcing.

If surf zone sampling is assumed to be dominant, then Guza and Bowen (1976) suggest that edge waves are most likely to survive if their offshore length scales are large compared to the width of the surf zone. This simply favours low frequencies and high mode numbers but does not provide a selection mechanism for a particular frequency.

Ball (1967) suggested that particular offshore beach topographies can select favoured edge wave modes, the cut-off modes. Huntley (1976) finds field evidence for cut-off modes from Hell's Mouth Bay. However, this cut-off requires the beach profile to flatten in water which is not "deep" for the edge wave, a requirement not met by Martinique with its approximately plane profile. For the large longshore wavelengths inferred for these low frequencies, the longshore beach topography provides the most significant constraint on possible length scales and hence edge wave frequencies. The headland and reef at the beach ends, and the second reef two thirds of the distance along the beach suggests  $b=953m$  as a fundamental longshore length scale for the beach (figure 2). As free waves reflected between end walls on a sloping beach are necessarily edge waves, an obvious model to consider is one based on the superposition of standing edge waves. Requiring that an integral number  $m$  of half-wavelengths fit into  $b$ , and using equation 3, we find

$$f = \left( \frac{g \tan \beta}{4\pi b} \right)^{\frac{1}{2}} (m(2n+1))^{\frac{1}{2}}$$

$$= 4.04 \times 10^{-3} (m(2n+1))^{\frac{1}{2}}$$

The combination of  $m=2$ ,  $n=1$  provides an excellent fit, predicting a frequency of .0099 hz compared to the observed frequency of .01 hz. However, it should be noted that equation (5) describes a whole suite of possible edge waves which could fit the beach. Addition of surf zone damping constraints as described previously and forcing as discussed by Gallagher (1971) and extended by Bowen and Guza (1978) does not alter the picture significantly enough to produce the narrow 100 second peak observed. So the present theoretical picture is one of a fairly broad-banded spectrum with the only features being "valleys" at frequencies where the non-dimensional offshore distance of the instrument  $\chi_1 = \sigma^2 x_1 / g\beta$  corresponds to an edge node (see figure 1).

Further evidence that topographic constraints are basic to the frequency selection is provided by data taken at approximately the same location on Martinique Beach in July of the previous year when the beach was steeper, with  $\beta=0.05$ . On that day, a narrow, energetic peak centered at 62 seconds was observed (figure 14). If the same length scale is responsible for both the 62 and the 100 second peaks, then, using equation (3), the ratio of edge wave periods for a change in beach slope should be

$$\frac{T_1}{T_2} = \left( \frac{\beta_2}{\beta_1} \right)^{\frac{1}{2}} = 0.63$$

This ratio is almost exactly satisfied for the two peaks indicating that in the face of different incident conditions and a different offshore profile, the edge wave adjusts to give the same wavelength, presumably because of longshore topographic trapping.

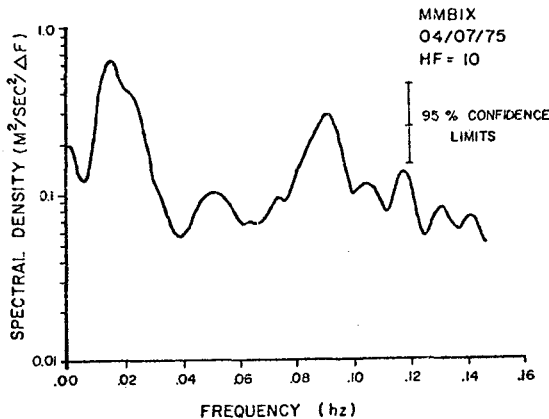


Fig. 14

Onshore velocity spectrum taken from the same location on 4 July 1975. Note the strong 62 second peak.

CONCLUSIONS:

A field experiment recording wave velocities during both calm and storm conditions showed a dramatic jump in infragravity (0.003-0.03 Hz) energy during the storm. At the height of the storm, infragravity waves accounted for 84% of all spectral energy. This low frequency dominance sheds doubt on the relevance of the simple, visually-observed, wave statistics in understanding surf zone dynamics.

A strong 100 second peak appeared in the onshore velocity spectra of all flowmeters near the beginning of the storm. This peak remained dominant and consistent in frequency through two further tides despite significant changes in the incident wave climate. Longshore topographic constraints are probably important in providing the lengthscale necessary for frequency selection, although the addition of forcing and damping constraints to the topographic model produces a fairly broad-banded theoretical spectrum, not the narrow 100 second peak observed.

REFERENCES

- Ball, F. K., Edge waves in a ocean of finite depth. *Deep Sea Res. Oceanogr. Abstr.*, 14, 79-88, 1967.
- Bowen, A. J. and R. T. Guza, Edge waves and surf beat. *J. Geophys. Res.*, 83, 1913-1920, 1978.
- Bowen, A. J., and D. L. Inman, Edge waves and crescentic bars. *J. Geophys. Res.*, 76, 8662-8671, 1971.
- Gallagher, B., Generation of surf beat by non-linear wave interactions. *J. Fluid Mech.*, 49, 1-20, 1971.
- Guza, R. T. and A. J. Bowen, Resonant interactions for waves breaking on a beach. *in* Proceedings of the 15th International Conference on Coastal Engineering, pp. 560-579, American Society of Civil Engineers, New York, 1976.
- Huntley, D. A., Long-period waves on a natural beach. *J. Geophys. Res.* 81, 6441-6449, 1976.
- Huntley, D. A. and A. J. Bowen, Comparison of the hydrodynamics of steep and shallow beaches. *in* Nearshore Sediment Dynamics and Sedimentation, edited by J. Hails and A. Carr, Wiley Interscience, London, pp. 69-110, 1975.
- Longuet-Higgins, M. S. and R. W. Stewart, Radiation stress in water waves: a physical discussion, with applications. *Deep Sea Res. Oceanogr. Abstr.*, 11, 529-562, 1964.
- Munk, W. H., Surf beats. *Eos Trans. AGU*, 30, 849-854, 1949.
- Schalk, M., Study of nearshore bottom profiles east and southwest of Point Barrow, Alaska; comparison of profiles and the barrier islands in the Point bay and Plover Island areas. *Arctic Inst. North America, Projects ONR 217, 241, Final Rept.*, 16 pp, unpub. manuscript.

- Short, A. D., Multiple offshore bars and standing waves. *J. Geophys. Res.*, 80, 3838-3840, 1975.
- Suhayda, J. N., Standing waves on beaches. *J. Geophys. Res.*, 72 (21), 3065-3071, 1974a.
- Suhayda, J. N., Determining infragravity wave spectra. in *International Symposium on Ocean Wave Measurements and Analysis*, v. 1, 54-63, 1974b.
- Tucker, M. J., Surf beats: Sea waves of 1 to 5 minute period. *Proc. Roy. Soc., Ser. A*, 202, 565-573, 1950.